

Effects of vertical confinement on gelation and sedimentation of colloids

Azaima Razali,^{1,2,3} Christopher J. Fullerton,^{4,5} James Hallett,^{1,2} Robert L. Jack,⁵ and C. Patrick Royall^{1,2,6,7, a)}

¹⁾*H.H. Wills Physics Laboratory, Tyndall Avenue, Bristol, BS8 1TL, UK*

²⁾*Centre for Nanoscience and Quantum Information, Tyndall Avenue, Bristol, BS8 1FD, UK*

³⁾*Kulliyyah of Science, International Islamic University Malaysia, Jalan Istana, Bandar Indera Mahkota, 25200 Kuantan, Pahang, Malaysia*

⁴⁾*Laboratoire Charles Coulomb, UMR 5221, Université Montpellier, Montpellier, France*

⁵⁾*Department of Physics, University of Bath, Bath, BA2 7AY, UK*

⁶⁾*School of Chemistry, University of Bristol, Cantock's Close, Bristol, BS8 1TS, UK*

⁷⁾*Department of Chemical Engineering, Kyoto University, Kyoto 615-8510, Japan*

We consider the sedimentation of a colloidal gel under confinement in the direction of gravity. The confinement allows us to compare directly experiments and computer simulations, for the same system size. The reduced system size also leads to *qualitatively* different behaviour compared to bulk systems: in large systems gelation suppresses sedimentation, but for small systems sedimentation is *enhanced* relative to non-gelling suspensions. We map interaction parameters between a model experimental system (observed in real space) and computer simulations. Remarkably, we find that Brownian dynamics simulations in which hydrodynamic interactions between the particles are neglected exhibit sedimentation on the same timescale as an experiment. However the thickness of the “arms” of the gel is rather larger in the experiments, compared with the simulations. An analysis of local structure in the simulations showed similar behaviour to gelation in the absence of gravity.

I. INTRODUCTION

Non-equilibrium colloidal systems in gravitational fields display rich and challenging phenomena¹. Even the simplest colloidal system, hard spheres, exhibits a range of phenomena when the force of gravity is unleashed², due to the coupling between gravity, chemical potential^{3–6}, and solvent-mediated hydrodynamic interactions between the particles^{7–12}. Adding attractions between the colloids leads to very rich behaviour in quiescent systems (without gravity)^{1,13}. In particular, spinodal demixing can lead to a network of particles^{14–18} which undergoes dynamical arrest^{19,20}. The effective attractions in these colloidal systems are induced by the addition of non-absorbing polymer. The result is a mixture of three important components — colloids, polymers and solvent — whose equilibrium properties can be derived from an effective one-component system of colloids with attractive interactions. The interaction strength is determined by the polymer concentration^{21,22}.

The interplay of phase separation (which may be arrested) and sedimentation can result in novel structure-dynamical correlations^{1,5,6,13,23}. Among the most intriguing behaviour is that of gelation under gravity. In bulk systems, gelation typically suppresses sedimentation. This is because gelation (in the colloidal systems we consider) corresponds to the formation of a network of arrested material with finite zero-shear viscosity^{13,24–26}. This network can then support the weight of the colloids, suppressing sedimentation. Gels are therefore used extensively to extend the shelf-life of many products which

would otherwise sediment^{27,28}. Under some conditions the gel can persist for years²⁹, if the self-generated or gravitational stress is weaker than the yield stress³⁰, but gels very often undergo sedimentation^{31–33}. This is a poorly understood phenomenon and can sometimes be sudden in its onset — so-called delayed collapse³⁴.

Here we take a radical departure from previous work in the field. Hitherto, large experimental systems have been considered, where the particles are at least 10^5 times smaller than any linear dimension of the system, so there may be 10^{16} particles in the system^{13,34}. The associated experimental timescales are of the order of 10^7 diffusion times. Treating such large systems in a theoretical fashion is, at present, only possible with approximate approaches which make a one-dimensional solution to the height profile such as “batch settling”² and dynamic density functional theory³⁵. To the best of our knowledge such theoretical approaches have not been extended to consider systems which undergo gelation. This leaves computer simulation as a means to treat the problem of sedimenting gels, but the timescales (up to years) and the macroscopic system sizes are not accessible by direct simulation.

However, it is possible to conduct experiments in much smaller systems, glass capillaries. Figure 1 shows the difference between bulk systems (as reported previously^{13,34}) and the system size used in this work. Here the relevant linear dimension (the height) is of order 100 particle diameters which is amenable to computer simulation. Such small systems thus offer a testbed by which simulation may be compared with experiment. We employ Brownian dynamics simulations in which solvent-mediated hydrodynamic effects are included only at the one-body level (that is, Stokes drag), and hydrodynamic interactions between the particles are ne-

^{a)}Corresponding author: paddy.royall@bristol.ac.uk

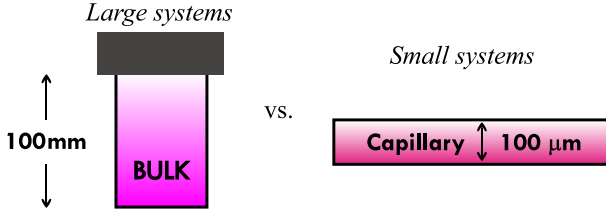


FIG. 1. A sketch showing the difference between typical experimental systems in previous work^{13,34}, and the system described here.

glected. Such interactions can have significant effects in sedimentation^{2,10–12,36} and in gelation^{37,38}. However, capturing them in simulations limits the accessible time scales and system sizes, and the Peclet numbers in these experiments are small, which we expect to reduce effects of hydrodynamic interactions. Hence, we compare the experiments with Brownian dynamics simulations, which are simple and computationally relatively inexpensive.

Remarkably, we find semi-quantitative agreement between experiment and simulation. Moreover, both reveal that sedimentation in such small systems is profoundly different from that in large systems. There, gelation inhibits sedimentation, where it finds use in prolonging the shelf-life of many products. Here in small systems quite the opposite behaviour is found: *gelation accelerates sedimentation*.

This paper is organised as follows. In section II, we describe our methodology by first defining the model system and interaction potential used in our experiments (in section II A), while details of the simulation model are given in II C. Next, in section III we report how the phase behaviour for our colloid-polymer system, sedimentation dynamics and interface of collapsing gels evolve in time for different interaction strengths. Then analysis of structures formed during the sedimentation process is documented in section III C. Finally, we conclude our discussions in section IV.

II. METHODS

A. Experiment

The experimental system is sterically stabilised polymethylmethacrylate (PMMA) with a diameter $\sigma = 460$ nm suspended in cis-decalin. The colloidal polydispersity is approximately 4% as determined with static light scattering. A colloidal gel was obtained by adding non-adsorbing polystyrene polymer with molecular weight $M_w = 3.46 \times 10^6$, leading to a polymer-colloid size ratio of $q = 2R_g/\sigma = 0.3$, where R_g is the polymer radius of gyration. The gravitational length was determined to be $\lambda_g = 6k_B T / (g\delta\rho\sigma^3) = 27.1\mu\text{m}$: here $\delta\rho$ is the density difference between the PMMA and the solvent, so λ_g is the height associated with a change of $k_B T$ in gravitational potential energy of a colloidal

particle. The Peclet number for sedimentation is then $Pe = \sigma/(2\lambda_g) = 8.51 \times 10^{-3}$. The colloid volume fraction is $\phi = 0.2$.

Each sample was transferred into a $100\mu\text{m}$ capillary and sealed with epoxy resin. We allowed the resin to set prior to imaging and data was taken after 5 minutes. The imaging of a z -stack of the entire capillary height was done using time-resolved confocal microscopy (Leica SP5). For each data set, the z -stack images were taken at intervals of approximately 8 minutes, for a duration of 20 hours. When reporting experimental data, we use the so-called polymer reservoir representation where the polymer concentration in the reservoir is related to that in the experiment by Widom particle insertion³⁹. The colloid volume fraction for each sample is extracted from the intensity measurements of the images obtained using the confocal microscope. These measurements were calibrated against homogeneous samples of known volume fraction, where there is a linear dependence of the measured intensity against colloid volume fraction.

B. Model and interaction potential

In the case that the polymers are much smaller than the colloids, the resulting mixture can be described by an Asakura-Oosawa (AO) model, which treats the polymer molecules as an ideal gas with hard interactions with the colloids, which themselves have hard interactions^{21,40–42}, can be well-described by the following expression.

$$u_{\text{AO}}(r) = \begin{cases} \infty & \text{for } r < \sigma \\ -\frac{k_B T \pi \sigma_p^3 z_p (1+q)^3}{6 q^3} & \text{for } \sigma \leq r < \sigma + \sigma_p \\ 0 & \text{for } r \geq \sigma + \sigma_p \end{cases} \quad (1)$$

The result is an effective interaction between the colloids of range $q\sigma$ and well-depth

$$u_{\text{AO}}^{\text{min}} = q^2 k_B T \rho_p \sigma^3 \frac{\pi(3+2q)}{12} \quad (2)$$

where ρ_p is the polymer number density.

For our parameters (size ratio $q = 0.3$ and polymer volume fraction $c_p/c_p^* = 4.8 \times 10^{-2} \text{g L}^{-1}$), the one-component mapping is expected to be rather accurate^{21,41}. As our unit of time, we use the Brownian time which we define as the typical time for a free colloidal particle to diffuse a distance comparable with its radius: $\tau_B = (\sigma/2)^2/6D = 0.0317\text{s}$, where $D = k_B T / (3\pi\eta\sigma)$ is the Stokes-Einstein diffusion constant, in which η is the solvent viscosity.

C. Simulation

Parameters and interactions. — As a simple way to mimic the experimental polydispersity (whose primary effect is to suppress crystallisation), we simulate a binary mixture of particles, with equal numbers of each species. The diameters of the two species are $\sigma_{AA} = 1.04\sigma$ and $\sigma_{BB} = 0.96\sigma$. We consider a total of $N = 60,000$ particles in a simulation box of size $L \times L \times L_z$ with $L = 28.025\sigma$ and $L_z = 200\sigma$, so that the volume fraction is $\phi = 0.2$, as in the experiment. All particles have mass m . The boundary conditions are periodic in the x and y directions: there are walls at $z = 0$ and $z = L_z$ that are described in detail below. The sample height L_z is comparable with the dimension of the capillary used in the experiment, and the lateral dimension L is comparable with the range over which experimental data was taken.

As a proxy for the AO potential between the colloids, we use a Morse potential

$$u_{\text{mor}}(r) = \epsilon_{\text{mor}} \left[e^{-2\alpha(r-\sigma_{ij})} - 2e^{-\alpha(r-\sigma_{ij})} \right], \quad (3)$$

where ϵ_{mor} is the depth of the attractive well, α sets the attraction range, and σ_{ij} is the position of the minimum of the interaction between particles of species i and j (which depends on the particle type). This potential accurately reproduces the behaviour of the AO system, including its higher-order local structure⁴². In contrast to the AO potential, the Morse potential is continuous, so that interparticle forces can be calculated, for use in computer simulations. We take $\alpha = 25.0\sigma^{-1}$ following⁴² and we use an additive mixing rule $\sigma_{AB} = (\sigma_{AA} + \sigma_{BB})/2 = \sigma$. The reduced well-depth $\epsilon_{\text{mor}}/(k_B T)$ is varied between 1.0 and 30.0.

The particles move in an external potential that includes the effects of gravity and of the confinement by the capillary. The gravitational potential energy of a particle at height z is $E_g(z) = z k_B T / \lambda_g$ with $\lambda_g = 60\sigma$, comparable with the experiment. The system is confined vertically by walls that are represented (for simplicity) by truncated and shifted Lennard-Jones potentials, as $u_{\text{wp}}(\Delta z) = 4\epsilon_{\text{wp}}[(\sigma_{\text{wp}}/\Delta z)^{12} - (\sigma_{\text{wp}}/\Delta z)^6]$ where Δz is the distance of the particle from the wall. The range of the potential is $\sigma_{\text{wp}} = 0.125\sigma$, comparable with the range of the Morse potential and the well-depth is $\epsilon_{\text{wp}} = 2\epsilon_{\text{mor}}$. The top wall (at $z = L_z$) is purely repulsive, so the potential is truncated and shifted at its minimum. The bottom wall (at $z = 0$) accounts for depletion interactions between colloids and the wall, and is truncated and shifted at $r = 2.4\sigma_{\text{wp}}$.

Dynamics and timescales. — Langevin (or Brownian) dynamics are implemented using the LAMMPS package⁴³. Particles have positions \mathbf{r}_i and velocities \mathbf{v}_i and the velocities evolve in time as

$$m \frac{d}{dt} \mathbf{v}_i = -\nabla_i V - \gamma \mathbf{v}_i + \sqrt{2\gamma k_B T} \boldsymbol{\xi}_i \quad (4)$$

where V is the total potential energy (including contributions from particle interactions, gravity, and the confin-

ing walls), while γ is a friction constant and $\boldsymbol{\xi}_i$ a random noise force. The friction constant sets the time scale for the decay of velocity correlations as $\tau_d = m/\gamma$.

There are a number of different time scales relevant for Langevin dynamics. As well as τ_d , there is a time scale $\tau_0 = \sqrt{m\sigma^2/k_B T}$ that is independent of the damping and sets the scale for particle velocities. Hence τ_0 is the natural time unit within the LAMMPS implementation. For colloids, the physical situation corresponds to an overdamped limit $\tau_d \ll \tau_0$. Here we take $\tau_d/\tau_0 = 0.1$, which is small enough to give the right qualitative behaviour — stronger damping would give a more accurate description but requires a more expensive numerical integration. The integration time step is $0.001\tau_0$. The single-particle diffusion constant is $D_0 = k_B T / \gamma$ so the Brownian time is $\tau_B = \sigma^2 / (24D) = \gamma \sigma^2 / (24k_B T) = \tau_0^2 / (24\tau_d)$, which for the parameters specified above corresponds to approximately 420 integration time steps.

Preparation of initial conditions. — The system is initialised in a well-mixed state, to mimic the experimental conditions. To achieve this, both the interparticle interactions and the interactions with the wall are truncated and shifted at their minima to achieve purely repulsive interactions. Particles are initialised in random positions, and a conjugate gradient minimisation (without gravitational forces) is used to remove particles that are overlapping. Then, the system is thermalised (still with purely repulsive interactions and without any gravitational forces) by evolving it for a time $50\tau_0$, leading to a homogeneous fluid configuration. These configurations are then used as initial conditions for the main simulations (including gravity and attractive interactions) for which results are shown below.

D. Mapping between experiment and simulation

To match the state points between the Morse potential used in simulation and the (approximately) Asakura-Oosawa interactions within the experiment, we used the extended law of corresponding states given by Noro and Frenkel⁴⁴. Identical well-depths and reduced second virial coefficients B_2^* (Eq. 5) are required in order to map the state points between simulations and experiments, where

$$B_2^* = \frac{B_2}{\frac{2}{3}\pi\sigma_{\text{eff}}^3}. \quad (5)$$

Here $B_2 = 2\pi \int_0^\infty [1 - \exp(-\beta u)] r^2 dr$ is the second virial coefficient and σ_{eff} is the effective diameter of a particle⁴⁵. For the AO potential, $\sigma_{\text{eff}} = \sigma$. For the Morse potential [Eq. 3], the effective diameter is fractionally smaller than σ , but this effect is very small for our parameters (around 1% of the diameter) and is neglected. For the simulation results reported here, we calculated the value of B_2^* associated with the relevant Morse potential, and then calculated the well-depth that would give the same value of B_2^* for an AO potential with $q = 0.3$.

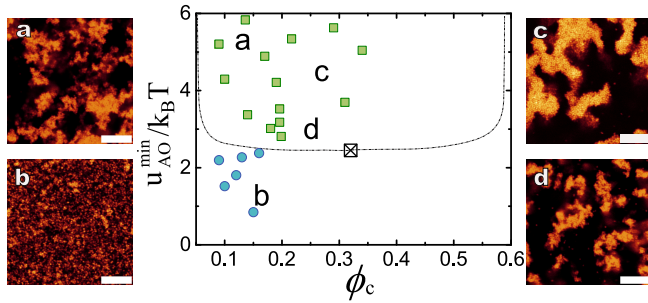


FIG. 2. Summary of the states observed in the experimental colloid-polymer mixture with $q = 0.3$, as a function of colloid volume fraction ϕ_c and attractive interaction strength $u_{\text{AO}}^{\text{min}}$. Green squares indicate gels and blue circles indicate homogeneous fluids. The \boxtimes is the critical point determined based on the reduced second virial coefficient B_2^* and critical isochore estimated from the literature^{46–48}. The scale bars represent $10 \mu\text{m}$.

In the following, simulation results are labelled by these effective AO well-depths, which are indicated by $u_{\text{AO}}^{\text{min}}$. These effective well-depths are comparable with (but do differ from) the well-depths ϵ_{mor} of the associated Morse potential.

III. RESULTS

A. Experimental phase behaviour

Fig. 2 summarises the behaviour of the experimental system, as a function of bond strength and colloid volume fraction. This behaviour is typical for colloid-polymer mixtures with size ratio $q = 0.3$. One expects a liquid-vapor critical point in this system whose position is determined from the extended law of corresponding states⁴⁴, shown here at $B_2^* = -1.5$. The critical isochore is estimated from the literature^{46–48}. In experimental samples, we see dynamically arrested gels for polymer concentrations higher than that for criticality. There is no sign of colloidal liquid-gas phase separation, presumably because the short range of the interaction results in dynamical arrest before phase separation can be completed. The polydispersity of the system prevents crystallisation on these time scales.

B. Global sedimentation dynamics

To analyse the time-evolution of the system, we first consider the sedimentation of the system as a whole, as illustrated in Fig. 3, for both simulation and experiment. At early times, one observes gelation as the formation of a percolating network of particles. At later times, particles can detach from the arms of the gel and diffuse through the solvent: this effect induces restructuring of the gel network, and eventual collapse^{33,34,49–51}. Here

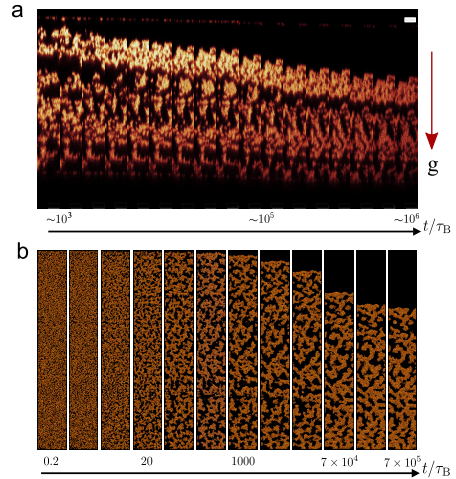


FIG. 3. Time-sequence of sedimenting gels captured from (a) experiment with $u_{\text{AO}}^{\text{min}} = 10 k_B T$ and (b) simulation corresponding to $u_{\text{AO}}^{\text{min}} = 7.1 k_B T$. The scale bar in (a) corresponds to $7.5 \mu\text{m}$. The snapshots of the experimental and simulation systems show regions of comparable size (measured in units of the colloid particle diameter σ).

the dynamics of the collapsing gel is recorded by taking 3d images in the confocal microscope which span the entire capillary at different times. Figure 3(a) shows a sequence of such confocal images as time progressed for a system with $u_{\text{AO}}^{\text{min}} = 10 k_B T$. From the confocal images, it is evident that the gel network is initially distributed throughout the whole capillary before falling under gravity at later times. The same qualitative behaviour is shown in the simulation data in Fig. 3(b).

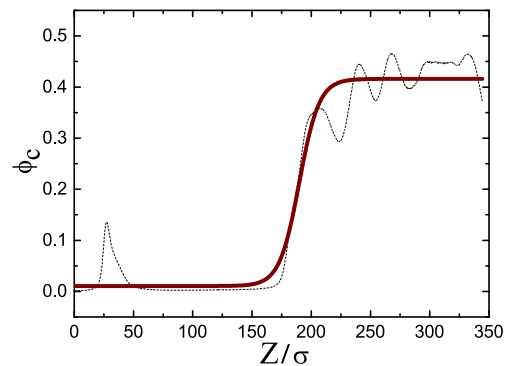


FIG. 4. Sedimentation profile $\phi(z)$ for an experimental system with $u_{\text{AO}}^{\text{min}} = 5 k_B T$ at time $t = 10^5 \tau_B$. Dashed line denotes experimental data, red line is a fit according to Eq. 6.

Given the behaviour shown in Fig. 3, it is natural to follow the time-dependence of the height of the collapsing gel. This is determined by plotting the local colloid volume fraction $\phi(z)$ as a function of height z , for each configuration in the trajectory as shown in figure 4. From the histogram, the interface is obtained by fitting a hy-

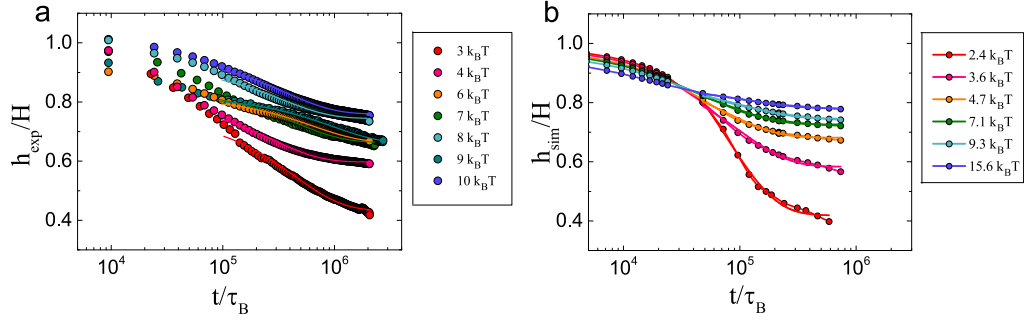


FIG. 5. Gel/vapour interface height plotted as a function of time. This height is estimated by fitting the function in (6) to a histogram of colloid density against height. Results from experiments are shown in (a); simulation results are shown in (b).

perbolic tangent to $\phi(z)$, as

$$\phi(z) = \phi_0 + \delta\phi \tanh\left(\frac{h-z}{\xi}\right). \quad (6)$$

Here ϕ_0 is the mean volume fraction in the regime we are fitting and $\delta\phi$ controls the change in volume fraction across the interface. There are two fitting parameters, the height of the gel h , and the interfacial width ξ .

The fitting parameter h is the height of the gel-vapour interface, which we plot in Fig. 5. We normalise by the total height of the system, as the tolerance of the capillaries used in the experiments leads to small changes (less than 5% in the value of H), thus we plot $h(t)/H$. Remarkably, the experiments and Brownian dynamics simulations exhibit sedimentation on a similar timescale, and the degree of collapse is similar, although the experiments exhibit a more gradual collapse on a somewhat longer timescale than do the simulations.

In the case where there are no attractive forces and the system does not gel, we show in Fig. 6 that, for our parameters, the sedimentation is negligible. To obtain this result, we consider *batch sedimentation*² of hard spheres for the same capillary height and a Péclet number $Pe = 0.01$, comparable with the experimental system. The rather small change in height shows that there is little or no significant sedimentation in a colloidal system without any polymer: we also verified this fact using simulations in the regime where attractions between particles are too weak to observe gelation.

In order to estimate a timescale for the sedimentation τ_{sed} , we heuristically fit the time-evolution of the interface height with an exponential decay,

$$h(t) = h_{t \rightarrow \infty} + h_{\text{drop}} e^{-t/\tau_{\text{sed}}} \quad (7)$$

where $h_{t \rightarrow \infty}$ is the interface height at long times and $h_{\text{drop}} = h(t=0) - h_{t \rightarrow \infty}$ is the amount by which the gel-vapour interface is estimated to fall at long times.

Fits according to Eq. 7 are shown in Fig. 5. We emphasise that this choice of fit is heuristic, and that the time-dependence of $h(t)$ is more complex than this simple exponential form, particularly for long times. Indeed we

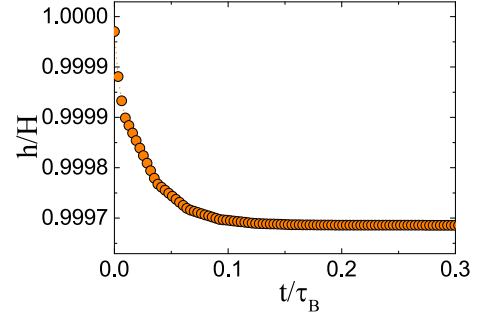


FIG. 6. Sedimentation of the colloidal system in the absence of polymer. Here the Péclet number $Pe = 0.01$, a magnitude larger than the Pe of our system. Data determined from batch sedimentation².

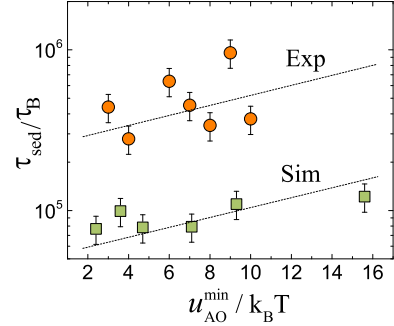


FIG. 7. Sedimentation timescale τ_{sed} as a function of interaction strength. Here we show both experimental and simulation data. Lines are to guide the eye.

expect that $h_{t \rightarrow \infty}$ may overestimate the interface height at long times, in the case of further sedimentation on scales beyond those we access here¹. The fits to the simulation data appear somewhat better than those for the experiments, suggesting some difference in the mechanism of sedimentation between experiment and simulation. The sedimentation time scales are also somewhat longer in the experiments. Note also that the exponential fits are more accurate when the attractive interactions are stronger and the amount of sedimentation is less.

Fig. 7 shows the sedimentation timescale τ_{sed} extracted from the fits. Two points here are worthy of note. Firstly, there is rather little change in the sedimentation timescale, an increase of a factor of two or three, despite the considerable change in interaction strength. Comparison with observations of bulk systems, where the interaction strength has a profound impact on the sedimentation timescale, especially in the case of delayed collapse³⁴, suggests that there may be a fundamental difference in mechanism between these confined systems and bulk measurements. Certainly the behaviour shown in Fig. 6 would be very different in bulk systems, where the system height is much greater than the gravitational length, so batch settling under gravity would lead to significant sedimentation even in the absence of attractive forces between colloids.

The discrepancy in time scales between simulation and experiments in Fig. 7 has several possible origins. The Morse potential used in the simulation has previously been shown to capture quite accurately the behaviour of this class of experimental system^{38,52,53}, and the AO model also matches such experiments³⁵. Moreover, the Morse and AO systems are also very similar to each other⁴², so we expect this aspect of the simulations to be reliable. The effects of continuous polydispersity in the experimental system are mimicked in the simulation by the use of a binary mixture: this is a coarse approximation but in the absence of significant crystallisation it seems unlikely to affect sedimentation time scales in this way. One possibility is that hydrodynamic interactions are important: these have been shown to have some influence in the time-evolution of gels in the absence of sedimentation^{37,38}. Another possibility, as we discuss below, is that the well-mixed initial conditions used in the simulations do not match the state of the colloidal suspensions at the beginning of the experiments.

C. Structural behaviour upon coarsening

Having analysed the height of the gel as a function of time, we now analyse the structure within the gel itself. This analysis takes two forms. First we consider the thickness of the network, which coarsens over time, as also happens in systems where sedimentation does not play an important role^{23,50,54}. To do this we determine the *chord length*¹⁹. We then perform a local structural analysis at the particle level on the simulation data using the topological cluster classification⁵⁵ and common neighbour analysis⁵⁶.

Chord length — To quantify the coarsening of the gel as it forms, we calculate the chord length¹⁹. First, the colloid density is coarse grained onto a grid of cells of side $\delta x = 0.5\sigma$. Let the position of the centre of cell α be R_α . Then, as an estimate of number of particles in its vicinity, define $n_\alpha = \sum_i f(|r_i - R_\alpha|)$ where the sum runs over all particles and $f(r) = e^{-r^2/\ell^2}$ is a (non-normalised) Gaussian smoothing function, with $\ell = 0.25\sigma$. If the cell

is within one of the arms of the gel then we expect n_α to be large; if the cell is in the vapour then n_α should be small. We identify each cell as either dense (gel) or dilute (vapour) by comparing n_α with a cutoff $n^* = 0.3$.

The lengths of all chords are then measured by moving in through the grid of cells in the x , y and z directions: each chord is a set of contiguous cells which all have $n_\alpha > 0.3$. Chords measured in the x and y directions are equivalent (as gravity acts in the z direction only), but we separate horizontal chords (aligned along the x and y directions) and vertical chords (aligned long z). To estimate the typical size of a horizontal chord, imagine choosing a particle at random and measuring the chord containing that particle. If the length of the j th horizontal chord is H_j then the average length of a horizontal chord chosen in this way is

$$L_H^m = \frac{\sum_j H_j^2}{\sum_j H_j} \quad (8)$$

where the superscript ‘m’ indicates that the average is *mass-weighted*. (That is, this average could equivalently be estimated by choosing particles at random and measuring the associated chords. On the other hand, averaging the length of a randomly chosen chord would give a different result. The mass-weighted average focusses attention on the chords which contain the majority of the particles and avoids numerical artefacts associated with large numbers of small chords.)

This typical chord length is shown in Fig. 8 for both experimental and simulation data. We see that the chord lengths for the experimental systems are significantly larger than those in the simulations. However, except for this difference in overall scale, the time-evolution in both experiment and simulation appears similar. It appears that the experiments are somehow forming larger domains at shorter times than the simulations, consistent with the qualitative results of Fig. 3.

There are several possibilities for this observation. The first is that the time-evolution is somehow different between the experiments and simulations, perhaps due to hydrodynamic interactions^{37,38}. Alternatively, the lateral size of the simulation box could influence the size of the networks formed. Previous simulation studies have emphasised the need for large systems in order to avoid finite size effects on the gel structure^{19,54}. (Note however that the lateral system size $L \approx 28\sigma$ is comparable with the range over which experimental data was taken.)

Another possibility is concerned with the experimental initial condition. In the experiments, we consider the start point $t = 0$ as the time at which the capillary is filled, from a parent suspension. The filling process breaks up any nascent gel network that may have formed within the parent suspension, and we assume that this has a similar effect to the random initial condition used in the simulations. In previous work with sedimentation on hard sphere systems, this approach was sufficient that the experiments and simulations began from essentially

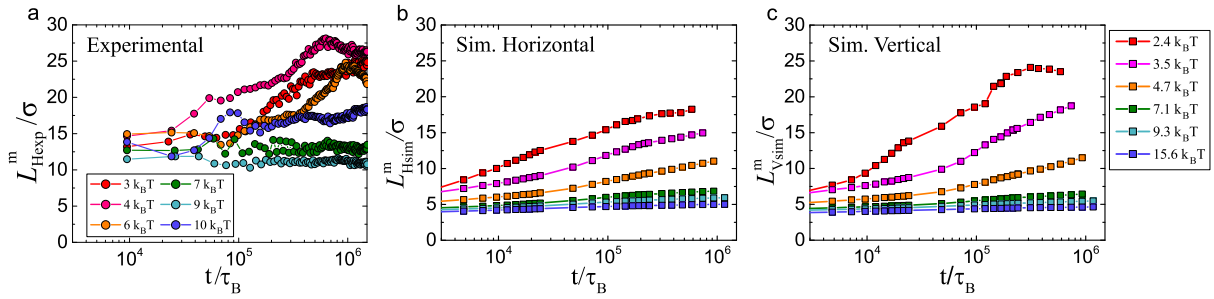


FIG. 8. Average chord length (mass weighted) measured (a) in the horizontal direction in the experimental system, (b) in the horizontal direction (perpendicular to the direction of gravity) (simulation), (c) in the vertical direction (the direction in which gravity acts) (simulation).

the same point^{10,35}. However, in systems with attractive forces, we cannot rule out that some form of residual structuring, for example small clusters, was already present in the experiment at the nominal time $t = 0$.

D. Local structural analysis

Gelation is accompanied by significant changes in local structure⁵². We therefore probe the local structure in our sedimenting gels, for which we consider two methods of analysis. The first is the Topological Cluster Classification (TCC)⁵⁵ and the second is a common neighbour analysis (CNA)⁵⁶. These measurements were performed as a function of the height within the gel but we found little vertical variation in the relative population of local structures (despite the density difference in the sedimentation profiles). In the following we therefore plot the population of local structures averaged across the whole system.

Topological cluster classification. — In this structural analysis, isolated clusters of particles were identified that represent energy minima of the Morse potential (with $\alpha = 25.0/\sigma$). Then, bond networks of the simulated gel structures were calculated using a modified Voronoi construction, and all 3, 4 and 5 membered shortest-path rings were identified within these bond networks⁵⁵ (we set the parameter $f_c = 0.82$). Then, local structures within the bond network that are topologically equivalent to the original energy minima were identified and enumerated. The clusters identified using the TCC are illustrated in Fig. 9, as are the proportions of particles that participate in clusters of each type. Since particles may be identified on more than one type of structure, the total across different types may exceed one.

Common neighbour analysis. — The common neighbour analysis (CNA)⁵⁶ offers a way to classify bonds. A bonded pair is classified based on how many mutual neighbours they share, and how these mutual neighbours are bonded. Of primary interest are 142 bonds, which are found in large numbers in both the HCP and FCC crystals. (These 142-bonds⁵⁷ include both the 1421 and

1422 bonds of the original scheme⁵⁶). Figure 9 shows the average number of 142 bonds that a particle participates in for different well depths. Here, a particle participates in a 142 bond if it is one of the two particles forming the central bonded pair.

In Fig. 9 we plot a number of local structures known to be important in gelation^{52,53,58}. The data reveals a number of observations. The first is that all three state points exhibit similarities in their behaviour. At short times, there are few structures. Upon condensation, (the first stage of gelation), local structures form, beginning with the 5-membered bitetrahedron. This is similar to previous work in quiescent (non-sedimenting) systems⁵⁸, and we note that the tetrahedron is the simplex for spheres in 3d, so its prevalence at early times is expected. Again, similar to previous studies^{58,59}, we see a tendency to the 10-membered defective icosahedron at longer times.

Upon weak quenching Fig. 9(a), we find a considerable degree of crystallisation at longer times, as observed previously in related systems⁵⁷. Moreover, the appearance of crystalline order as measured by the TCC occurs up to an order of magnitude later in time than the emergence of crystalline 142-bonds as measured by the CNA. While these 142-bonds are associated with crystallisation, they represent a lower degree of local order than the 13 particle clusters that are identified as fcc/hcp in the TCC analysis. Increasing the strength of attractions leads to a suppression of crystallisation in the timescales accessible here, consistent with previous work^{48,52,53,57,58}.

In summary, given the change in state parameters, the local structural evolution of our sedimenting gels is not markedly different to that of quiescent gels⁵⁸. We note that while we expect the binary system used in these simulations to mimic the large-scale properties of the experiments, the presence of only two component types does have the potential to influence local structure (and crystallisation) when compared to the continuous polydispersity of experimental systems. Note however that in contrast to both the experimental and simulation systems considered here, monodisperse systems crystallise much more easily, leading to rather different behaviour^{58,60}.

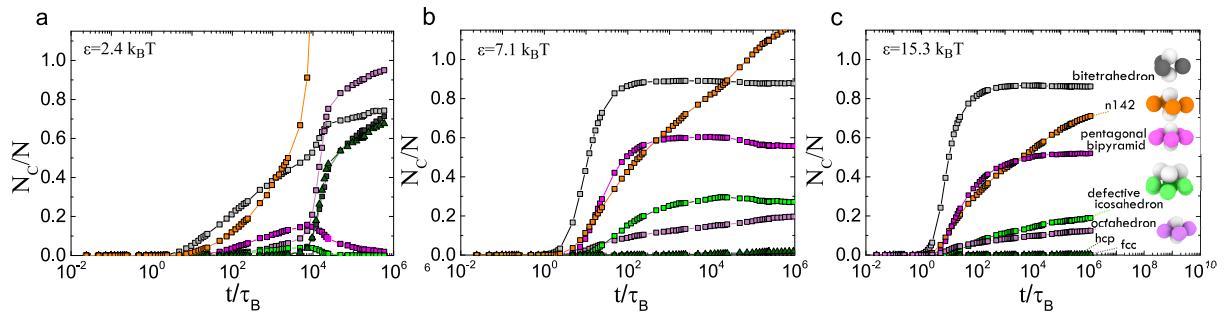


FIG. 9. Time-evolution of the local structure in simulations. We consider three state points for which the effective AO well depths are $\epsilon_{\text{eff}} = 2.4, 7.1$ and $15.3 k_B T$. The ‘142’ clusters are detected by the common neighbour analysis, other structures are found with the topological cluster classification (TCC). For TCC clusters, we show the fraction of particles (N_C/N) that participate in at least one cluster of the relevant type. Hence one clearly has clearly $N_C/N \leq 1$. For 142 clusters, N_C/N is the average number of 142-bonds in which a particle participates, so one may have $N_C/N > 1$ (indeed for a perfect fcc crystal one would have $N_C/N = 12$).

IV. CONCLUSIONS

We have carried out a combined experimental and simulation study of colloidal gels undergoing sedimentation. The vertical confinement of these systems profoundly affects their sedimentation behaviour. In particular, in these small systems where the gravitational height is comparable to the system size, sedimentation is absent except when particle interactions are strong enough to drive gelation. (Recall Fig. 6 which shows that sedimentation is insignificant in a hard-sphere colloidal system with comparable parameters to those considered here.)

Our Brownian dynamics simulations provide a reasonable description of the time-evolution of the system. This is possible due to a careful mapping of the interaction parameters between experiment and simulation. The agreement between simulation and experiment is notable, given that the simulations do not feature hydrodynamic interactions. The major differences in behaviour between simulation and experiment are that the simulations appear to sediment a little faster than the experiments. Structural analysis on the dimensions of the gel network suggest that the experiments are rather coarser. This may be related to some intrinsic difference in the dynamics, or to a finite size effect in the simulations, or to incomplete homogenisation of the experimental system prior to gelation.

We have also considered the local structure of the simulated gels. We find that it is rather similar to structural evolution found in quiescent (non-sedimenting) systems. Recalling from Fig. 3(b) that the system clearly condenses into a percolating network before any significant sedimentation has occurred, it seems that the main changes in the local structure of the system occur on short time scales that are decoupled from sedimentation. Figure 9 is also consistent with this interpretation.

Finally, we note that simulation studies such as these might provide a basis by which coarse-grained theoretical models might be developed, which might be able to tackle

truly macroscopic systems. This would be valuable since macroscopic phenomena such as delayed gel collapse³⁴ are not accessible in these small (confined) systems, and are therefore beyond the reach of direct simulation. For this reason, development of such coarse-grained models would form a major step forward in the understanding and modelling of these important materials.

ACKNOWLEDGMENTS

CPR acknowledges the Royal Society, the European Research Council (ERC consolidator grant NANOPRS, project number 617266), the Japan Society of the Promotion of Science (JSPS) and Kyoto University SPIRITS fund for financial support and EPSRC grant code EP/H022333/1 for the provision of a confocal microscope. AR is grateful to the Malaysia’s Ministry of Education (MOE) for the financial support and thanks R. Pinchaipat & F. Turci for the assistance in data analysis. CJF and RLJ acknowledge support from the UK Engineering and Physical Science Research Council (EPSRC) through grants EP/I003797/1 and EP/L001438/1.

- ¹R. Piazza, S. Buzzaccaro, and E. Secchi, “The unbearable heaviness of colloids: facts, surprises, and puzzles in sedimentation,” *J Phys.: Condens Matter* **24**, 284109 (2012).
- ²W. B. Russel, D. Saville, and W. Schowalter, *Colloidal Dispersions* (Cambridge Univ. Press, Cambridge, 1989).
- ³R. Piazza, T. Bellini, and V. Degiorgio, “Equilibrium sedimentation profiles of screened charged colloids: A test of the hard sphere equation of state,” *Phys. Rev. Lett.* **25**, 4267–4270 (1993).
- ⁴C. Royall, D. Aarts, and H. Tanaka, “Fluid structure in colloid-polymer mixtures: the competition between electrostatics and depletion,” *J. Phys.: Condens. Matter* **17**, S3401–S3408 (2005).
- ⁵S. Buzzaccaro, R. Rusconi, and R. Piazza, ““sticky” hard spheres: Equation of state, phase diagram, and metastable gels,” *Phys. Rev. Lett.* **99**, 098301 (2007).
- ⁶M. Leocmach, R. C. P., and H. Tanaka, “Novel zone formation due to interplay between sedimentation and phase ordering,” *EuroPhys. Lett.* **89**, 38006 (2010).

- ⁷P. Segre, H. E., and P. Chaikin, “Long-range correlations in sedimentation,” *Phys. Rev. Lett.* **79**, 2574–2577 (1997).
- ⁸P. N. Segre, F. Liu, P. Umbanhowar, and D. A. Weitz, “An effective gravitational temperature for sedimentation,” *Nature* **409**, 594–597 (2001).
- ⁹J. T. Padding and A. A. Louis, “Hydrodynamic and brownian fluctuations in sedimenting suspensions,” *Phys. Rev. Lett.* **93**, 220601 (2004).
- ¹⁰A. Wysocki, C. P. Royall, R. Winkler, G. Gompper, H. Tanaka, A. van Blaaderen, and H. Löwen, “Direct observation of hydrodynamic instabilities in driven non-uniform colloidal dispersions,” *Soft Matter* **5**, 1340–1344 (2009).
- ¹¹A. Moncho Jorda, A. A. Louis, and J. T. Padding, “Effects of inter-particle attractions on colloidal sedimentation,” *Phys Rev Lett* **104** (2010).
- ¹²C. Wysocki, A. Rath, A. V. Ivlev, K. R. Sutterlin, H. M. Thomas, S. Khrapak, S. Zhdanov, V. E. Fortov, A. M. Lipaev, V. I. Molotkov, O. F. Petrov, H. Lowen, and G. E. Morfill, “Kinetics of fluid demixing in complex plasmas: Role of two-scale interactions,” *Phys. Rev. Lett.* **105**, 045001 (2010).
- ¹³W. C. K. Poon, “The physics of a model colloid-polymer mixture,” *J. Phys.: Condens. Matter* **14**, R859–R880 (2002).
- ¹⁴N. A. M. Verhaegh, D. Asnaghi, H. N. W. Lekkerkerker, M. Giglio, and L. Cipelletti, “Transient gelation by spinodal decomposition in colloid-polymer mixtures,” *Physica A* **242**, 104–118 (1997).
- ¹⁵H. Tanaka, “Viscoelastic model of phase separation in colloidal suspensions and emulsions,” *Phys. Rev. E* **59**, 6842 (1999).
- ¹⁶S. Manley, H. Wyss, K. Miyazaki, J. Conrad, V. Trappe, L. Kaufman, D. Reichman, and D. Weitz, “Glasslike arrest in spinodal decomposition as a route to colloidal gelation,” *Phys. Rev. Lett.* **95**, 238302 (2005).
- ¹⁷P. J. Lu, E. Zaccarelli, F. Ciulla, A. B. Schofield, F. Sciortino, and D. A. Weitz, “Gelation of particles with short-range attraction,” *Nature* **435**, 499–504 (2008).
- ¹⁸E. Zaccarelli, P. J. Lu, F. Ciulla, D. A. Weitz, and F. Sciortino, “Gelation as arrested phase separation in short-ranged attractive colloid-polymer mixtures,” *J Phys.: Condens Matter* **20**, 494242 (2008).
- ¹⁹V. Testard, L. Berthier, and W. Kob, “Influence of the glass transition on the liquid-gas spinodal decomposition,” *Phys. Rev. Lett.* **106**, 125702 (2011).
- ²⁰P. Chaudhuri and L. Berthier, “Ultra-long-range dynamic correlations in a microscopic model for aging gels,” *ArXiv* , 1605.09770 (2016).
- ²¹M. Dijkstra, R. van Roij, and R. Evans, “Effective interactions, structure, and isothermal compressibility of colloidal suspensions,” *J. Chem. Phys.* **113**, 4799–4807 (2000).
- ²²C. Likos, M. Schmidt, H. Löwen, M. Ballauff, D. Pötschke, and P. Lindner, “Soft interaction between dissolved flexible dendrimers: theory and experiment,” *Macromolecules* **34**, 2914–2920 (2001).
- ²³R. Zia, B. Landrum, and W. B. Russel, “A micro-mechanical study of coarsening and rheology of colloidal gels: Cage building, cage hopping, and smoluchowski’s ratchet,” *J. Rhe* **58**, 1121–1157 (2014).
- ²⁴E. Zaccarelli, “Colloidal gels: Equilibrium and non-equilibrium routes,” *J. Phys.: Condens. Matter* **19**, 323101 (2007).
- ²⁵A. A. Coniglio, L. De Arcangelis, E. Del Gado, A. Fierro, and N. Sator, “Percolation, gelation and dynamical behaviour in colloids,” *J. Phys.: Condens. Matter* **16** (2004).
- ²⁶L. Ramos and L. Cipelletti, “Slow dynamics in glassy soft matter,” *Journal of Physics: Condensed Matter* **17**, R253–R285 (2005).
- ²⁷S. Manley, J. M. Skotheim, L. Mahadevan, and D. A. Weitz, “Gravitational collapse of colloidal gels,” *Phys Rev Lett* **94**, 218302 (2005).
- ²⁸R. D. MacBean, *Packaging and the Shelf Life of Yogurt*, edited by G. L. Robertson (CRC Press, 2009).
- ²⁹B. Ruzicka, E. Zaccarelli, L. Zulian, R. Angelini, M. Sztucki, A. Moussaid, T. Narayanan, and F. Sciortino, “Observation of empty liquids and equilibrium gels in a colloidal clay,” *Nature Materials* **10**, 56–60 (2010).
- ³⁰H. Tanaka, “Importance of many-body orientational correlations in the physical description of liquids,” *Faraday Discuss* **167**, 9–76 (2013).
- ³¹R. Piazza, “Settled and unsettled issues in particle settling,” *Rep. Prog. Phys.* **77** (2014).
- ³²L. Starrs, W. C. K. Poon, D. J. Hibberd, and M. M. Robins, “Collapse of transient gels in colloid-polymer mixtures,” *J Phys.: Condens Matter* **14**, 2485 (2002).
- ³³S. Buzzaccaro, E. Secchi, G. Brambilla, R. Piazza, and C. L., “Equilibrium concentration profiles and sedimentation kinetics of colloidal gels under gravitational stress,” *J. Phys.: Condens. Matter* **24** (2012).
- ³⁴P. Bartlett, L. Teece, and M. A. Faers, “Sudden collapse of a colloidal gel,” *Phys Rev E* **85** (2012).
- ³⁵C. P. Royall, A. A. Louis, and H. Tanaka, “Measuring colloidal interactions with confocal microscopy,” *J. Chem. Phys.* **127**, 044507 (2007).
- ³⁶C. Perez, A. , Moncho-Jorda, R. Hidalgo-Alvarez, and H. Casanova, “A comparative study on the effect of hydrodynamic interactions in the non-sequential deposition of concentrated colloidal dispersions: stochastic rotation dynamics and brownian dynamics simulations,” *Molecular Physics* **113**, 2857–3597 (2015).
- ³⁷A. Furukawa and H. Tanaka, “Key role of hydrodynamic interactions in colloidal gelation,” *Phys. Rev. Lett.* **104**, 245702 (2010).
- ³⁸R. C. P., J. Eggers, A. Furukawa, and T. H., “Probing colloidal gels at multiple length scales: The role of hydrodynamics,” *Phys Rev Lett* **114** (2015).
- ³⁹H. N. W. Lekkerkerker, W. C. K. Poon, P. N. Pusey, A. Stroobants, and P. B. Warren, “Phase-behavior of colloid plus polymer mixtures,” *Europhys. Lett.* **20**, 559–564 (1992).
- ⁴⁰A. Vrij, “Polymers at interfaces and interactions in colloidal dispersions,” *Pure Appl. Chem.* **48**, 471–483 (1976).
- ⁴¹M. Dijkstra, J. M. Brader, and R. Evans, “Phase behaviour and structure of model colloid-polymer mixtures,” *J. Phys.: Condens. Matter* **11**, 10079–10106 (1999).
- ⁴²J. Taffs, A. Malins, S. R. Williams, and C. P. Royall, “A structural comparison of models of colloid-polymer mixtures,” *J. Phys.: Condens. Matter* **22**, 104119 (2010).
- ⁴³“<http://lammps.sandia.gov>,”.
- ⁴⁴M. G. Noro and D. Frenkel, “Extended corresponding-states behavior for particles with variable range attractions,” *J. Chem. Phys.* **113**, 2941–2944 (2000).
- ⁴⁵J.-P. Hansen and I. Macdonald, *Theory of Simple Liquids* (Academic, London, 1976).
- ⁴⁶F. Lo Verso, R. L. C. Vink, D. Pini, and L. Reatto, “Critical behavior in colloid-polymer mixtures: Theory and simulation,” *Phys. Rev. E* **73**, 061407 (2006).
- ⁴⁷C. P. Royall, D. G. A. L. Aarts, and H. Tanaka, “Bridging length scales in colloidal liquids and interfaces from near-critical divergence to single particles,” *Nature Physics* **3**, 636–640 (2007).
- ⁴⁸S. Taylor, R. Evans, and C. P. Royall, “Temperature as an external field for colloid-polymer mixtures: “quenching” by heating and “melting” by cooling,” *J. Phys.: Condens. Matter* **24**, 464128 (2012).
- ⁴⁹E. Kilfoil, M. and Pashkovski, J. Masters, and D. A. Weitz, “Dynamics of weakly aggregated colloidal particles,” *Phil. Trans.* **361**, 753–766 (2003).
- ⁵⁰I. Zhang, C. P. Royall, M. A. Faers, and P. Bartlett, “Phase separation dynamics in colloid-polymer mixtures: the effect of interaction range,” *Soft Matter* **9**, 2076–2084 (2013).
- ⁵¹E. Secchi, S. Buzzaccaro, and R. Piazza, “Time-evolution scenarios for short-range depletion gels subjected to the gravitational stress,” *Soft Matter* **10**, 5296–5310 (2014).
- ⁵²C. Royall, S. Williams, T. Ohtsuka, and H. Tanaka, “Direct observation of a local structural mechanism for dynamic arrest,”

- Nature Materials **7**, 556 (2008).
- ⁵³C. P. Royall, S. R. Williams, T. Ohtsuka, and T. H., “Direct observation low-energy clusters in a colloidal gels,” American Institute of Physics Conference Proceedings **982**, 97 (2008).
- ⁵⁴V. Testard, L. Berthier, and W. Kob, “Intermittent dynamics and logarithmic domain growth during the spinodal decomposition of a glass-forming liquid,” J. Chem. Phys **140** (2014), doi: 10.1063/1.4871624.
- ⁵⁵A. Malins, S. R. Williams, J. Eggers, and C. P. Royall, “Identification of structure in condensed matter with the topological cluster classification,” J. Chem. Phys. **139**, 234506 (2013).
- ⁵⁶J. D. Honeycutt and H. C. Andersen, “Molecular dynamics study of melting and freezing of small lennard-jones clusters,” J. Phys. Chem. **91**, 4950–4963 (1987).
- ⁵⁷D. Klotz and R. L. Jack, “Predicting the self-assembly of a model colloidal crystal,” Soft Matter **7**, 6294–6303 (2011).
- ⁵⁸C. P. Royall and A. Malins, “The role of quench rate in colloidal gels,” Faraday Discuss. **158**, 301–311 (2012).
- ⁵⁹C. P. Royall, A. Malins, A. J. Dunleavy, and R. Pinney, “Strong geometric frustration in model glassformers,” submitted to J. Non-Cryst. Sol. (2014).
- ⁶⁰J. Doye and L. Meyer, “Mapping the Magic Numbers in Binary Lennard-Jones Clusters,” Physical Review Letters **95**, 1–4 (2005).